

Article

Optical Conductivity on Charge Order Transition in Organic Dirac Electron System α -(BEDT-TTF)₂I₃

Daigo Ohki ^{1,*}, Genki Matsuno ¹, Yukiko Omori ² and Akito Kobayashi ¹¹ Department of Physics, Nagoya University, Furo-cho, Chikusa-ku, Nagoya, 464-8602 Japan² Toyota College, National Institute of Technology, Eisei-cho 2-1, Toyota, 471-8525 Japan

* Correspondence: dohki@s.phys.nagoya-u.ac.jp

Abstract: The optical conductivity in the charge order phase is calculated in the extended Hubbard model describing an organic Dirac electron system α -(BEDT-TTF)₂I₃ using the mean field theory and the Nakano-Kubo formula. A peak structure due to interband excitation being characteristic in two-dimensional Dirac electron system is found above the charge order gap. It is shown that the peak structure originates from the Van Hove singularities of the conduction and valence bands, where those singularities are located at a saddle point between two Dirac cones in momentum space. The frequency of the peak structure exhibits drastic change in the vicinity of the charge order transition.

Keywords: Dirac electron; charge order; optical conductivity; organic conductor; α -(BEDT-TTF)₂I₃

1. Introduction

An organic conductor α -(BEDT-TTF)₂I₃ has attracted many interests, since it exhibits a transition between the charge order (CO)[1–6] and the massless Dirac electron (massless DE) [7–14] as hydrostatic pressure, P , increases. Recently, strong electron correlation effects have been revealed in both the CO[15] and the massless DE[16–19] in spin fluctuations. Thus electron correlation effects in transport phenomena have been also expected, especially in crossover region between the CO and the massless DE.

It has been observed that the optical gap determined by the optical conductivity decreases monotonously as P increases and reaches almost zero at about $P_c = 12$ kbar[20,21], while the resistivity gap reaches almost zero at about 7 kbar[22]. In order to explain such metallic behavior in the presence of the CO gap, metallic channels owing to edges and domain walls in the CO have been studied using the extended Hubbard model[23–26]. It has been shown that the massive DE phase with the gapless edge states emerges in the intermediate region between the massless DE phases and the trivial CO. Although the CO gap induced by the inversion symmetry breaking exists in both the massive DE phase and the trivial CO, a pair of Dirac cones with a finite gap at incommensurate momentum, $\pm k_D$, merges at a time reversal invariant momentum (TRIM) at the transition between these two phases[11,14,27,28]. Such a drastic change in the band structure is expected to give rise to a characteristic in the optical conductivity.

In the present paper, the optical conductivity is calculated in the band structure determined by the mean-field theory in the extended Hubbard model for the two dimensional electron system in the organic conductor α -(BEDT-TTF)₂I₃, where the CO transition is controlled by the nearest-neighbor Coulomb repulsion, V_a . It is shown that a peak structure emerges above the CO gap in the optical conductivity. The frequency of the peak structure, ω_{peak} , owing to interband excitation between two Van Hove singularities in the conduction and valence bands, rapidly moves as a nonmonotonic function of V_a , while the frequency of the CO gap, ω_{CO} , increases monotonically as V_a increases. Those Van Hove singularities originate from the saddle points between two Dirac cones. The optical conductivity exhibits a characteristic strong peak when two Dirac cones merge in the presence of a large CO gap.

This paper is described as follows. An extended Hubbard model for two dimensional electron system in α -(BEDT-TTF)₂I₃, the mean field theory, and the optical conductivity are described in section 2. Numerical results are shown in section 3. Section 4 and 5 are devoted to discussion and summary.

2. Formulation

The extended Hubbard model[1,2] has been used in theoretical studies for α -(BEDT-TTF)₂I₃, in order to take the on-site Coulomb repulsion, U , and the nearest-neighbor Coulomb repulsions, $V_{\alpha\beta}$, into account.

$$\begin{aligned}
 H = & \sum_{(i\alpha,j\beta),\sigma} (t_{(i\alpha,j\beta)} a_{i\alpha\sigma}^\dagger a_{j\beta\sigma} + \text{h.c.}) \\
 & + \sum_{i\alpha} U a_{i\alpha\uparrow}^\dagger a_{i\alpha\downarrow}^\dagger a_{i\alpha\downarrow} a_{i\alpha\uparrow} \\
 & + \sum_{(i\alpha;j\beta)} \sum_{\sigma,\sigma'} V_{i\alpha j\beta} a_{i\alpha\sigma}^\dagger a_{j\beta\sigma'}^\dagger a_{j\beta\sigma'} a_{i\alpha\sigma},
 \end{aligned} \quad (1)$$

where $a_{i\alpha\sigma}$ and $t_{(i\alpha,j\beta)}$ represent the annihilation operators and the transfer energies with unit cells i, j , spins σ , and sublattices $\alpha, \beta = A, A', B$ and C of α -(BEDT-TTF)₂I₃.

Hereafter, the energies are given in eV. The tight binding model for α -(BEDT-TTF)₂I₃[29–33] is shown in Fig. 1(a). The sublattice A and A' are equivalent due to the inversion symmetry in the massless DE phase. The transfer energies given by the first-principle calculation[32]: $t_{b1} = 0.1241, t_{b2} = 0.1296, t_{b3} = 0.0513, t_{b4} = 0.0152, t_{a1} = -0.0267, t_{a2} = -0.0511, t_{a3} = 0.0323, t'_{a1} = 0.0119, t'_{a3} = 0.0046$, and $t'_{a4} = 0.0060$. The nearest neighbor interaction V_a in the stacking direction is used for controlling the CO transition, because this is the most sensitive as a function of P [34–36], while we treat $U = 0.4$ and $V_b = 0.05$ as constants. The temperature $T = 0.001$ is fixed in the present paper. The lattice constants, k_B and \hbar are taken as unity. The system size in numerical calculations is $N_L = 500$.

The mean-field Hamiltonian H_{MF} [10] is

$$H_{\text{MF}} = \sum_{\mathbf{k}\alpha\beta\sigma} \tilde{\epsilon}_{\alpha\beta\sigma}(\mathbf{k}) a_{\mathbf{k}\alpha\sigma}^\dagger a_{\mathbf{k}\beta\sigma}, \quad (2)$$

$$\tilde{\epsilon}_{\alpha\beta\sigma}(\mathbf{k}) = \phi_{\alpha\sigma} \delta_{\alpha\beta} + \epsilon_{\alpha\beta}(\mathbf{k}), \quad (3)$$

$$\phi_{\alpha\sigma} = U_\alpha \langle n_{\alpha-\sigma} \rangle + \sum_{\beta'\sigma'} V_{\alpha\beta'} \langle n_{\beta'\sigma'} \rangle, \quad (4)$$

$$\epsilon_{\alpha\beta}(\mathbf{k}) = \sum_{\delta} t_{\alpha\beta} e^{i\mathbf{k}\cdot\delta}, \quad (5)$$

where $\phi_{\alpha\sigma}$ is the Hartree potential, $\langle n_{\alpha\sigma} \rangle = \langle a_{i\alpha\sigma}^\dagger a_{i\alpha\sigma} \rangle$ is the electron number, and δ is a vector between unit cells. The energy eigenvalues $\xi_{\gamma\sigma}(\mathbf{k})$ and the wave functions $\Phi_{\alpha\gamma\sigma}(\mathbf{k})$ are given by

$$\sum_{\beta} \tilde{\epsilon}_{\alpha\beta\sigma}(\mathbf{k}) \Phi_{\beta\gamma\sigma}(\mathbf{k}) = \xi_{\gamma\sigma}(\mathbf{k}) \Phi_{\alpha\gamma\sigma}(\mathbf{k}), \quad (6)$$

with the band index $\gamma = 1, 2, 3, 4$. The conduction and valence bands correspond to $\xi_{1\sigma}(\mathbf{k})$ and $\xi_{2\sigma}(\mathbf{k})$, respectively, since the Fermi energy is located between these two bands. The electron number $\langle n_{\alpha\sigma} \rangle$ is given by

$$\langle n_{\alpha\sigma} \rangle = \sum_{\mathbf{k}\gamma} |\Phi_{\alpha\gamma\sigma}(\mathbf{k})|^2 f(\xi_{\gamma\sigma}(\mathbf{k})), \quad (7)$$

where the Fermi distribution function is $f(\xi_{\gamma\sigma}(\mathbf{k})) = 1/(\exp[(\xi_{\gamma\sigma}(\mathbf{k}) - \mu)/k_B T] + 1)$ with the chemical potential μ determined so that the bands are 3/4-filled.

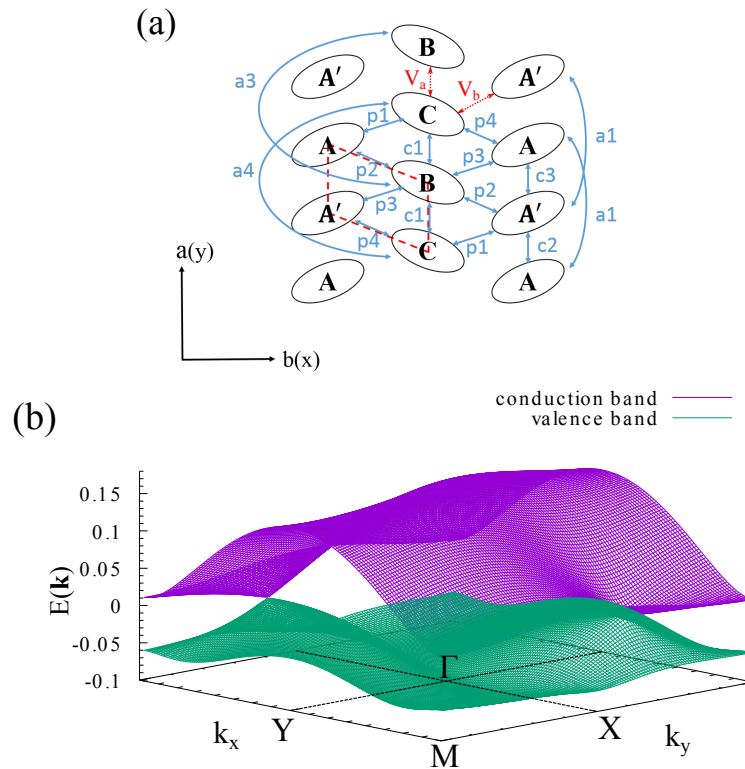


Figure 1. Schematic figure of a unit cell with transfer energies, on-site Coulomb repulsion U and the nearest-neighbor Coulomb repulsions, V_a and V_b (a). The conduction band (purple) and valence band (green) in the massive DE phase for $V_a = 0.18$ (b).

63 The Green function $G_{\alpha\beta\sigma}(\omega, \mathbf{k})$ and the density of state $\rho(\omega)$ are given by

$$G_{\alpha\beta\sigma}(\omega, \mathbf{k}) = \sum_{\gamma} \frac{\Phi_{\alpha\gamma\sigma}^* \Phi_{\beta\gamma\sigma}}{\hbar\omega - (\xi_{\gamma\sigma}(\mathbf{k}) - \mu) + i\delta'} \quad (8)$$

$$\begin{aligned} \rho(\omega) &= \frac{1}{N_L} \sum_{\mathbf{k}\alpha\sigma} \left(-\frac{1}{\pi} \text{Im} G_{\alpha\alpha\sigma}(\omega, \mathbf{k}) \right) \\ &= \frac{1}{N_L} \sum_{\mathbf{k}\alpha\gamma\sigma} \delta(\hbar\omega - \xi_{\gamma\sigma}(\mathbf{k})) |\Phi_{\gamma\alpha\sigma}(\mathbf{k})|^2, \end{aligned} \quad (9)$$

64 where N_L is the number of lattice points.

65 The optical conductivity is calculated by the Nakano-Kubo formula based on linear response
66 theory. It is represented by

$$\sigma(\omega) = \frac{1}{i\omega} [K(\omega) - K(0)], \quad (10)$$

$$K(\omega) = -\frac{1}{N_L} \left(\frac{e}{\hbar} \right)^2 \sum_{\mathbf{k}\gamma\gamma'\sigma} |\mathbf{v}_{\gamma\gamma'\sigma}(\mathbf{k})|^2 \frac{f(\xi_{\gamma\sigma}(\mathbf{k})) - f(\xi_{\gamma'\sigma}(\mathbf{k}))}{\xi_{\gamma\sigma}(\mathbf{k}) - \xi_{\gamma'\sigma}(\mathbf{k}) + \omega + i\delta'} \quad (11)$$

67 where the velocity matrix $\mathbf{v}_{\gamma\gamma'\sigma}$ is calculated by

$$\mathbf{v}_{\gamma\gamma'\sigma}(\mathbf{k}) = \sum_{\alpha\beta} \Phi_{\alpha\gamma\sigma}^*(\mathbf{k}) v_{\alpha\beta\sigma}(\mathbf{k}) \Phi_{\beta\gamma'\sigma}(\mathbf{k}), \quad (12)$$

$$v_{\alpha\beta\sigma}(\mathbf{k}) = \frac{1}{\hbar} \frac{\partial}{\partial \mathbf{k}} \epsilon_{\alpha\beta\sigma}(\mathbf{k}). \quad (13)$$

68 3. Results

69 Figure 1(b) shows the conduction and valence bands in the massive DE phase. There is a pair of
70 massless Dirac cones at incommensurate momenta, $\pm k_D$. The Fermi energy is located at the degenerate
71 points of the two bands. There are several saddle points at the TRIMs near the Fermi energy, *e. g.*,
72 the M-point in the conduction band (Mc-VHS), the M-point in the valence band (Mv-VHS), and the
73 Y-point in the valence band (Yv-VHS).

74 The optical conductivities at several V_a are shown in Fig. 2(a). These values are divided by
75 the universal conductivity $\sigma_0 = \pi e^2/2h$ [37]. In the massless DE phase for $V_a = 0.18$, the optical
76 conductivity almost reaches a universal constant for $T < \omega < \Lambda$, where $\Lambda \cong 0.01$ is a energy scale of
77 the linear dispersion as shown in previous studies for the massless DE [37–40]. When $V > V_a^{c1} = 0.198$,
78 a frequency of the CO gap, ω_{CO} , increases as V_a increases as shown in Fig. 2(b), where ω_{CO} is defined
79 as a flexion point of the shoulder structure in the optical conductivity. It is found that a peak structure
80 appears above ω_{CO} and its frequency, ω_{peak} , rapidly decreases as V_a increases for $V_a < V_a^{c2} = 0.212$,
81 which is defined by the merging of the Dirac cones in the conduction band [25,26]. ω_{peak} rebounds
82 after falling to ω_{CO} , and the optical conductivity shows a strong peak. Those two frequencies exhibits
83 asymptotic behavior for $V_a > V_a^{c2}$.

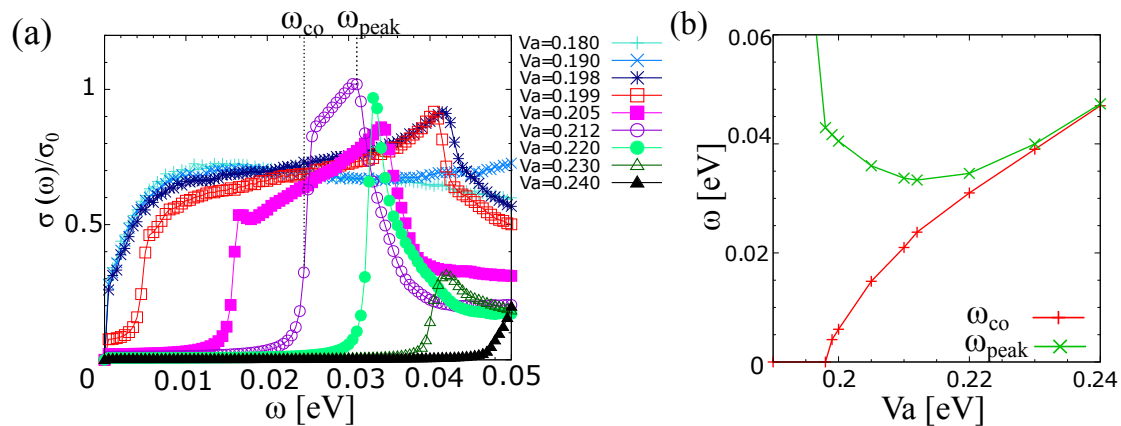


Figure 2. The optical conductivities divided by the universal conductivity $\sigma_0 = \pi e^2/2h$ [37] for $V_a = 0.180, 0.190, 0.198, 0.199, 0.205, 0.212, 0.220, 0.230, 0.240$ (a). ω_{CO} and ω_{peak} for $V_a = V_a^{c2} = 0.212$ are shown in (a). V_a -dependences of ω_{CO} and ω_{peak} are shown in (b). A characteristic peak structure is found near the CO transition in the extended Hubbard model describing the organic Dirac electron system α -(BEDT-TTF)₂I₃.

84 Figure 3 shows the density of states $\rho(\omega)$, where the Fermi energy is defined as zero. When
85 $V_a < V_a^{c1}$, there is a valley due to the Dirac cones. A CO gap, ω_{CO} , opens at the Fermi energy for
86 $V > V_a^{c1}$. There are several Van Hove singularities (VHS) due to saddle points of the conduction
87 and valence bands (see Fig. 1(b)). Here we pay attention to VHS at the M-point in the conduction
88 band (Mc-VHS) and that in the valence band (Mv-VHS), respectively. The Mc-VHS stays an energy
89 for $V_a < V_a^{c2}$. Its energy rapidly increases and the peak structure disappears for $V_a > V_a^{c2}$, since it is
90 absorbed by the upper edge of the CO gap, owing to the merging of the Dirac cones in the conduction
91 band as shown in Fig. 4. The Mv-VHS, on the other hand, moves very rapidly until it reaches the
92 lower edge of the CO gap at V_a^{c2} . The Mv-VHS and the lower edge of the CO gap exhibits asymptotic
93 behavior for $V_a > V_a^{c2}$. An energy difference between the Mc-VHS and Mv-VHS coincides with ω_{peak}
94 in the optical conductivity shown in Fig. 2(a). Other VHSs, *e. g.*, VHS at the Y-point in the valence
95 band (Yv-VHS), show completely different behavior as V_a increases.

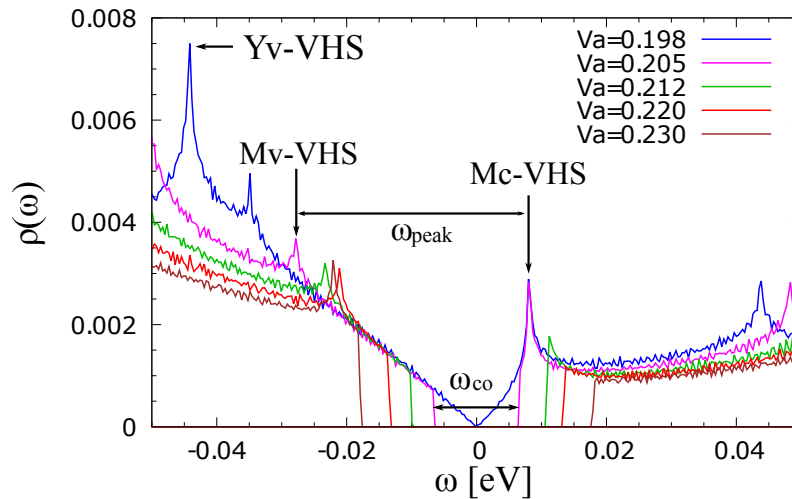


Figure 3. The density of states $\rho(\omega)$ for $V_a = 0.198, 0.205, 0.212, 0.220, 0.230$. The origin of the peak structure in the optical conductivity is identified.

96 In order to analyze the behavior of ω_{peak} and ω_{CO} , the band structure is intensively examined in
 97 Fig. 4. Both Mc-VHS and Mv-VHS exist at the M-point (the saddle point) between two Dirac cones.
 98 The Dirac cones in the conduction band (the purple band) merge at the M-point at V_a^{c2} in the presence
 99 of large CO gap as shown in Figs. 4(b) and 4(e), leading to the absorption of the Mc-VHS into the
 100 upper edge of the CO gap. On the other hand, the massive Dirac cones in the valence band (the green band)
 101 do not merge against relatively larger V_a as shown in Figs. 4(c) and 4(f), since the Dirac cones
 102 are tilted[11,12]. Thus the Mv-VHS and the lower edge of the CO gap shows asymptotic behavior.

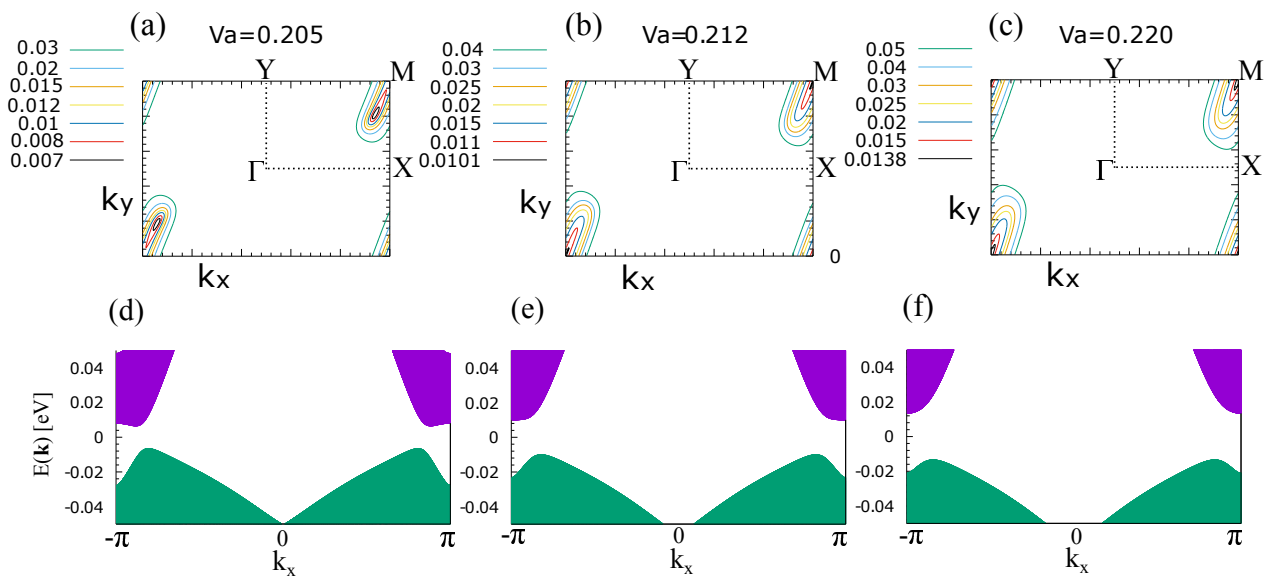


Figure 4. The contour plots of the conduction band for $V_a = 0.205$ (a), $V_a = V_a^{c2} = 0.212$ (b), and $V_a = 0.220$ (c). The band structures as a function of k_x for $V_a = 0.205$ (d), $V_a = V_a^{c2} = 0.212$ (e), and $V_a = 0.220$ (f), where the CO gaps open between the conduction bands (the purple bands) and the valence bands (the green bands). Tilting of the Dirac cones causes electron-hole asymmetric behavior as the CO gap increases.

103 4. Discussion

104 The drastic change of the optical conductivity near CO transition is characterized not only the CO
 105 gap, but also the peak structure as shown in Fig. 2(a) and 2(b). By careful analysis on the $\rho(\omega)$ shown

106 in Fig. 3 and band structure shown in Fig. 4, it is elucidated that the origin of the peak structure is the
 107 VHSs at the M-points between two tilted Dirac cones. The nonmonotonic V_a -dependence of ω_{peak} is
 108 due to both the merging of the Dirac cones with the CO gap and the tilting of the Dirac cones. Those
 109 characteristic may be measured in the low frequency region of the optical conductivity[20], which
 110 can provide many important information on existence, merging, and tilting of the two-dimensional
 111 massive Dirac electrons in the CO phase.

112 5. Conclusions

113 The optical conductivity in the vicinity of the CO transition has been investigated using the
 114 Nakano-Kubo formula and the mean-field theory in the extended Hubbard model describing the Dirac
 115 electrons in α -(BEDT-TTF)₂I₃. It has been found that a peak structure above the CO gap emerges due to
 116 the two dimensional Dirac cones. It has been also shown that the drastic change of the peak structure
 117 in the vicinity of the CO transition indicates the merging of the massive Dirac electrons.

118 **Acknowledgments:** This work was supported by MEXT/JSPJ KAKENHI under Grant Noes 15K05166 and
 119 15H02108.

120 **Author Contributions:** A. K. and Y. O. conceived and designed the theories; D. O. and G. M. performed the
 121 numerical calculation and analyzed the data; D. O. and A. K. wrote the paper.

122 **Conflicts of Interest:** The authors declare no conflict of interest.

123 Abbreviations

124 The following abbreviations are used in this manuscript:

125	DE	Dirac electron
	CO	charge order
	VHS	Van Hove singularity
	DOS	density of states
126	TRIM	time reversal invariant momentum
	Mc-VHS	Van Hove singularity at the M-point in the conduction band
	Mv-VHS	Van Hove singularity at the M-point in the valence band
	Yv-VHS	Van Hove singularity at the Y-point in the valence band

127 References

- 128 1. H. Kino and H. Fukuyama, T. Interrelationship among Electronic States of α -(ET)₂I₃, (ET)₂MHg(SCN)₄ and
 129 κ -(ET)₂X. *J. Phys. Soc. Jpn.* **1995**, *64*, 4523, 10.1143/JPSJ.64.4523.
- 130 2. H. Seo, T. Charge Ordering in Organic ET Compounds. *J. Phys. Soc. Jpn.* **2000**, *69*, 805, 10.1143/JPSJ.69.805.
- 131 3. C. Hotta, T. Classification of Quasi-Two Dimensional Organic Conductors Based on a New Minimal Model.
 132 *J. Phys. Soc. Jpn.* **2003**, *72*, 840, 10.1143/JPSJ.72.840.
- 133 4. T. Takahashi, T. ¹³C-NMR studies of charge ordering in organic conductors. *Synth. Met.* **2003**, *26*, 133-134,
 134 10.1016/S0379-6779(02)00404-6.
- 135 5. H. Seo, C. Hotta, and H. Fukuyama, T. Toward Systematic Understanding of Diversity of Electronic Properties
 136 in Low-Dimensional Molecular Solids. *Chem. Rev.* **2004**, *104*, 5005, 10.1021/cr030646k.
- 137 6. T. Kakiuchi, Y. Wakabayashi, H. Sawa, T. Takahashi, and T. Nakamura, T. Charge Ordering
 138 in α -(BEDT-TTF)₂I₃ by Synchrotron X-ray Diffraction. *J. Phys. Soc. Jpn.* **2007**, *76*, 113702,
 139 10.1143/JPSJ.76.113702.
- 140 7. K. Kajita, T. Ojio, H. Fujii, Y. Nishio, H. Kobayashi, A. Kobayashi, and R. Kato, T. Magnetotransport
 141 Phenomena of α -Type (BEDT-TTF)₂I₃ under High Pressures. *J. Phys. Soc. Jpn.* **1992**, *61*, 23,
 142 10.1143/JPSJ.61.23.
- 143 8. N. Tajima, M. Tamura, Y. Nishio, K. Kajita, and Y. Iye, T. Transport Property of an Organic Conductor
 144 α -(BEDT-TTF)₂I₃ under High Pressure - Discovery of a Novel Type of Conductor -. *J. Phys. Soc. Jpn.* **2000**,
 145 *69*, 543-551, 10.1143/JPSJ.69.543.

- 146 9. K. Ishikawa, M. Hirata, D. Liu, K. Miyagawa, M. Tamura, and K. Kanoda, T. Spin excitations in the
147 quasi-two-dimensional charge-ordered insulator α -(BEDT-TTF)₂I₃ probed via ¹³C NMR. *Phys. Rev. B* **2016**,
148 94, 085154, PhysRevB.94.085154.
- 149 10. A. Kobayashi, S. Katayama, K. Noguchi, and Y. Suzumura, T. Superconductivity in Charge Ordered Organic
150 Conductor α -(ET)₂I₃ Salt-. *J. Phys. Soc. Jpn.* **2004**, 73, 3135, 10.1143/JPSJ.73.3135.
- 151 11. S. Katayama, A. Kobayashi, and Y. Suzumura, T. Pressure-Induced Zero-Gap Semiconducting State in
152 Organic Conductor α -(BEDT-TTF)₂I₃ Salt. *J. Phys. Soc. Jpn.* **2006**, 75, 054705, 10.1143/JPSJ.75.054705.
- 153 12. A. Kobayashi, S. Katayama, Y. Suzumura, and H. Fukuyama, T. Massless Fermions in Organic Conductor.
154 *J. Phys. Soc. Jpn.* **2007**, 76, 034711, 10.1143/JPSJ.76.034711.
- 155 13. K. Kajita, Y. Nishio, N. Tajima, Y. Suzumura, and A. Kobayashi, T. Molecular Dirac Fermion Systems
156 -Theoretical and Experimental Approaches-. *J. Phys. Soc. Jpn.* **2014**, 83, 072002, 10.7566/JPSJ.83.072002.
- 157 14. M. O. Goerbig, J.-N. Fuchs, G. Montambaux, and F. Piéchon, T. Tilted anisotropic Dirac cones in quinoid-type
158 graphene and α -(BEDT-TTF)₂I₃. *Phys. Rev. B* **2008**, 78, 045415, 10.1103/PhysRevB.78.045415.
- 159 15. Y. Tanaka and M. Ogata, T. Correlation Effects on Charge Order and Zero-Gap State in the Organic Conductor
160 α -(BEDT-TTF)₂I₃. *J. Phys. Soc. Jpn.* **2016**, 85, 104706, 10.7566/JPSJ.85.104706.
- 161 16. M. Hirata, K. Ishikawa, K. Miyagawa, M. Tamura, C. Berthier, D. Basko, A. Kobayashi, G. Matsuno and K.
162 Kanoda, T. Observation of an anisotropic Dirac cone reshaping and ferrimagnetic spin polarization in an
163 organic conductor. *Nat. Commun.* **2016**, 7, 12666, 10.1038/ncomms12666.
- 164 17. G. Matsuno and A. Kobayashi, T. Effect of Interband Fluctuation on Spin Susceptibility in Molecular Dirac
165 Fermion System α -(BEDT-TTF)₂I₃. *J. Phys. Soc. Jpn.* **2016**, 86, 014705, 10.7566/JPSJ.86.014705.
- 166 18. M. Hirata, K. Ishikawa, G. Matsuno, A. Kobayashi, K. Miyagawa, M. Tamura, C. Berthier, K. Kanoda, T.
167 Anomalous spin correlations and excitonic instability of interacting 2D Weyl fermions. *Science* **2017**, 358,
168 1403, 10.1126/science.aan5351.
- 169 19. G. Matsuno and A. Kobayashi, submitted.
- 170 20. R. Beyer, A. Dengl, T. Peterseim, S. Wackerow, T. Ivek, A.V. Pronin, D. Schweitzer, and M. Dressel, T.
171 Pressure-dependent optical investigations of α -(BEDT-TTF)₂I₃: Tuning charge order and narrow gap towards
172 a Dirac semimetal. *Phys. Rev. B* **2016**, 93, 195116, 10.1103/PhysRevB.93.195116.
- 173 21. T. Ivek, B. Korin-Hamzić, O. Milat, S. Tomić, C. Clauss, N. Drichko, D. Schweitzer, and M. Dressel, T.
174 Electrodynamic response of the charge ordering phase: Dielectric and optical studies of α -(BEDT-TTF)₂I₃.
175 *Phys.Rev.B* **2011**, 83, 165128, 10.1103/PhysRevB.83.165128.
- 176 22. D. Liu, K. Ishikawa, R. Takehara, K. Miyagawa, M. Tamura, and K. Kanoda, T. Insulating nature of
177 strongly correlated massless Dirac fermions in an organic crystal. *Phys.Rev.Lett.* **2016**, 116, 226401,
178 10.1103/PhysRevLett.116.226401.
- 179 23. Y. Hasegawa and K. Kishigi, T. Edge States in the Three-Quarter Filled System, α -(BEDT-TTF)₂I₃.
180 *J. Phys. Soc. Jpn.* **2011**, 80, 054707, 10.1143/JPSJ.80.054707.
- 181 24. Y. Omori, G. Matsuno, and A. Kobayashi, T. Edge States in Molecular Solid α -(BEDT-TTF)₂I₃: Effects of
182 Electron Correlations. *JPSConf. Proc.* **2014**, 1, 012119, 10.7566/JPSJ.1.012119.
- 183 25. G. Matsuno, Y. Omori, T. Eguchi, and A. Kobayashi, T. Topological Domain Wall and Valley Hall Effect
184 in Charge Ordered Phase of Molecular Dirac Fermion System α -(BEDT-TTF)₂I₃ *J. Phys. Soc. Jpn.* **2016**, 85,
185 094710, 10.7566/JPSJ.85.094710.
- 186 26. Y. Omori, G. Matsuno, A. Kobayashi, T. Longitudinal Conductivity on Edge and Domain Wall Molecular
187 Dirac Electron System α -(BEDT-TTF)₂I₃. *J. Phys. Soc. Jpn.* **2017**, 86, 074708, 10.7566/JPSJ.86.074708.
- 188 27. G. Montambaux, F. Piéchon, J.-N. Fuchs, and M. O. Goerbig, T. Merging of Dirac points in a two-dimensional
189 crystal. *Phys. Rev. B* **2009**, 80, 153412, 10.1103/PhysRevB.80.153412.
- 190 28. G. Montambaux, F. Piéchon, J.-N. Fuchs, and M. O. Goerbig, A universal Hamiltonian for the
191 motion and the merging of Dirac cones in a two-dimensional crystal. *Eur. Phys. J. B* **2009**, 72, 509,
192 10.1140/epjb/e2009-00383-0
- 193 29. T. Mori, A. Kobayashi, Y. Sasaki, H. Kobayashi, G. Saito, and H. Inokuchi, T. BAND STRUCTURES OF TWO
194 TYPES OF (BEDT-TTF)₂I₃. *Chem. Lett.* **1984** 957, 10.1246/cl.1984.957.
- 195 30. T. Mori, H. Mori, and S. Tanaka, T. Structural Genealogy of BEDT-TTF-Based Organic Conductors II. Inclined
196 Molecules: θ , α , and κ Phases. *Bull. Chem. Soc. Jpn.* **1999**, 72, 179, 10.1246/bcsj.72.179.

- 197 31. R. Kondo S. Kagoshima, and J. Harada, T. Crystal structure analysis under uniaxial strain at low temperature
198 using a unique design of four-axis x-ray diffractometer with a fixed sample. *Rev. Sci. Instrum.* **2005**, *76*,
199 093902, 10.1063/1.2001607.
- 200 32. H. Kino and T. Miyazaki, T. First-Principles Study of Electronic Structure in α -(BEDT-TTF)₂I₃ at Ambient
201 Pressure and with Uniaxial Strain. *J. Phys. Soc. Jpn.* **2006**, *75*, 034704, 10.1143/JPSJ.75.034704.
- 202 33. S. Ishibashi, T. Tamura, M. Kohyama, and K. Terakura, T. Ab Initio Electronic-Structure Calculations for
203 α -(BEDT-TTF)₂I₃. *J. Phys. Soc. Jpn.* **2006**, *75*, 015005, 10.1143/JPSJ.75.015005.
- 204 34. A. Kobayashi, S. Katayama and Y. Suzumura, T. Superconductivity in Charge Ordered Metal for
205 Quasi-Two-Dimensional Organic Conductor. *J. Phys. Soc. Jpn.* **2005**, *74*, 2897, 10.1143/JPSJ.74.2897.
- 206 35. A. Kobayashi S. Katayama, and Y. Suzumura, T. Theoretical study of the zero-gap organic conductor
207 α -(BEDT-TTF)₂I₃. *Sci. Tech. Adv. Mater.* **2009**, *10*, 024309, 10.1088/1468-6996/10/2/024309.
- 208 36. N. Tajima and K. Kajita, T. Experimental study of organic zero-gap conductor α -(BEDT-TTF)₂I₃.
209 *Sci. Tech. Adv. Mater.* **2009**, *10*, 024308, 10.1088/1468-6996/10/2/024308.
- 210 37. T. Stauber, N. M. R. Peres, and A. K. Geim, T. Optical conductivity of graphene in the visible region of the
211 spectrum. *Phys.Rev.B* **2008**, *78*, 085432, 10.1103/PhysRevB.78.085432.
- 212 38. V. P. Gusynin, S. G. Sharapov, and J. P. Carbotte, T. Unusual Microwave Response of Dirac Quasiparticles in
213 Graphene. *Phys.Rev.Lett.* **2006**, *96*, 256802, 10.1103/PhysRevLett.96.256802.
- 214 39. Y. Suzumura, I. Proskurin, and M. Ogata, T. Dynamical Conductivity of Dirac Electrons in Organic
215 Conductors. *J.Phys.Soc.Jpn.* **2014**, *83*, 094705, 10.7566/JPSJ.83.094705.
- 216 40. Y. Suzumura, I. Proskurin, and M. Ogata, T. Reflectance of Dirac electrons in organic conductor. *J.Phys. :
217 Conf.Ser.* **2015**, *603*, 012011, 10.1088/1742-6596/603/1/012011.